Meteorological controls on evapotranspiration over a coastal salt marsh ecosystem under tidal influence

Ying Huang[a], Haiqiang Guo[b], Xuelong Chen[c], Zihan Chen[a], Christiaan van der Tol[d], Yunxuan Zhou[a], Jianwu Tang[a,e,*]

[a] State Key Laboratory of Estuarine and Coastal Research, Institute of Eco-Chongming, East China Normal University, Shanghai, China
[b] Ministry of Education Key Laboratory for Biodiversity Science and Ecological Engineering, Fudan University, Shanghai, China
[c] Key Laboratory of Tibetan Environment Changes and Land Surface Processes, Institute of Tibetan Plateau Research, Chinese Academy of Sciences, Beijing, China
[d] Faculty of Geo-Information Science and Earth Observation, University of Twente, Enschede, the Netherlands
[e] The Ecosystems Center, Marine Biological Laboratory, Woods Hole, MA, USA

ARTICLE INFO

ABSTRACT

Elucidating evapotranspiration (ET) patterns and drivers is of crucial importance for better understanding water and energy cycles. However, multiple controls on ET at coastal ecosystems that are subject to subdaily tidal flooding have not yet received attention. In this study, we investigated the response of ET to meteorological variables including photosynthetically active radiation (PAR), air temperature (T_a), vapour pressure deficit (VPD), and wind speed (WS) under semidiurnal tidal influence from hourly to seasonal timescales, on the basis of 3-year eddy-covariance (EC) measurements over a tidal salt marsh ecosystem of the Yangtze Delta. Our results show that, as with most terrestrial ecosystems, PAR is a major control on ET in this coastal salt marsh ecosystem at hourly, diel, and multiday timescales. However, the semidiurnal tides co-control ET with meteorological variables, forming a complex ET pattern at the hourly and subdaily scales. In the daytime, ET was primarily driven by PAR and VPD, whereas during the night, WS and friction velocity dominated the ET variability. We also found that wind direction fundamentally changed the nature of the interactions of ET with other variables. Moreover, tidal inundation suppressed ET and changed its sensitivities to PAR, T_a, VPD, and WS, a process that was especially obvious when offshore winds prevailed. The tidal flooding can affect ET directly through altering surface energy partitioning or plant metabolic activity, and indirectly through influencing meteorological conditions such as T_a and VPD. By explicitly considering the influence of tidal dynamics, this study revealed the significance in quantifying the ET contributions in coastal ecosystems to global water, carbon and energy cycles.

1. Introduction

Evapotranspiration (ET) represents the combined flux associated with two different pathways of water vaporization, namely abiotic water evaporation and biotic leaf transpiration. As a major component of the energy and water cycles, ET drives mass transport and energy exchange in the soil-vegetation-atmosphere interface (Katul et al., 2012). Additionally, ET is the key process linking the water and energy cycles with other biochemical processes (e.g. carbon and nutrient cycles) (Wagle et al., 2015; Zhou et al., 2015), thereby playing an important part in the Earth's soil-vegetation-atmosphere-climate system. However, ET is probably the least understood component in the hydrologic budget (Jung et al., 2010; Lettenmaier and Famiglietti, 2006), since it is multi-controlled by, for instance, physical and canopy

physiological processes that are responsive to environmental conditions such as precipitation, light, air temperature (T_a), humidity, and soil water content.

Recent advances in micrometeorological instrumentation have demonstrated the advantage in quantifying ET in a variety of ecosystems, such as forests (Igarashi et al., 2015; Zhu et al., 2014; Tang et al., 2006), grassland (Ma et al., 2015; Qiu et al., 2011), cropland (Bezerra et al., 2012; Lei and Yang, 2010), wetland (Liljedahl et al., 2011), shrubland (Odongo et al., 2016), and desert (Unland et al., 1996). The eddy-covariance (EC) technique is considered as an important tool for providing a direct and robust means to measure continuous latent heat fluxes (LE) and thus ET (Wilson and Baldocchi, 2000; Baldocchi, 2003). During the last four decades, over 800 EC flux towers and several associated global and regional networks (e.g., FLUXNET, AsiaFlux,

---

EuroFlux, AmeriFlux, and ChinaFlux) have been established all over the world, leading to a better understanding of ET variabilities and their main environmental controls in a variety of terrestrial ecosystems. However, most of these studies on ET have focused on upland ecosystems or freshwater wetlands. Although LE affected by the tides from coastal wetlands has been reported in a few studies, none of them explicitly explored the multiple controls on ET over tidal wetlands (Guo et al., 2010; Harazono et al., 1998; Moffet et al., 2010). Up to date, coastal ecosystems that are subject to subdaily tidal flooding have not received attention in studying their ET patterns and drivers.

Coastal salt marshes are unique ecosystems located in the coastal intertidal zone between land and ocean, and are among the most productive, most economically important, and most vulnerable ecosystems on the planet (Goulden et al., 2007; Kirwan and Megonigal, 2013). A number of studies have been conducted in characterizing water and energy fluxes and elucidating the mechanisms in wetlands, such as peatland (Admiral et al., 2006; Admiral and Lafleur 2007; Moore et al., 2013), prairie wetland (Burba et al., 1999a,b), and coastal tundra (Liljedahl et al. 2011; Harazono et al., 1998). However, investigating environmental controls on ET at saltmarsh wetlands featured by semi-diurnal/diurnal tides are still very limited. EC towers were established more recently at tidal wetlands than inland ecosystems (Baldocchi, 2014; Forbrich et al., 2015; Guo et al., 2009; Kathilankal et al., 2008). The multiple controls of meteorological variables (e.g., precipitation, light, temperature, humidity, soil water content) on ET over tidal saltmarsh ecosystems are complicated by the unique features of coastal wetlands, for instance, the tidal dynamics and strong horizontal advection.

ET in the salt marsh ecosystem takes place from soil pores, intercepted water on leaves, and tidal water (evaporation), and from stomata of saltmarsh plants (transpiration), and the energy cost in the processes can be from the sun, usually by solar radiation, or indirectly taken from the air. ET processes are controlled both by atmospheric demand for water and soil moisture supply, and the former is associated with, for instance, available energy, air temperature (T_a), vapour pressure deficit (VPD), and wind speed (WS), whereas the latter mainly refers to soil water availability (Monteith and Unsworth, 2013). The turbulence is responsible for the transport of heat and water vapour through the surface boundary layer, and the aerodynamic resistance that is related to WS and friction velocity (u_*) modulates the water vapour transfer rates. On the other hand, ET is directly linked to vegetation physiology, as transpiration is controlled by stomatal conductance that represents the regulation of the leaf stomata on the water vapor flow (Eichelmann et al., 2018; Dolman et al., 2014; Raupach, 1995).

Since coastal tidal salt marshes are regularly flooded and drained by saltwater brought in by the tides, the soil tends to be saturated, regardless of precipitation. Soil moisture is supposed to have very limited constraint on ET variations, which is rather different from inland ecosystems. On the other hand, the effect of VPD, which represents atmospheric demand for water, on ET is also rather unique in tidal saltmarsh wetlands. As VPD is relatively low in tidal saltmarsh wetlands compared to, for instance, arid and semi-arid regions, it may mainly control ET by a direct atmospheric constraint (evaporation will be constrained because of the high vapor pressure in the atmosphere), rather than an indirect constraint through an increased bulk surface resistance (Liljedahl et al., 2011). Therefore, it is likely that elevated VPD barely raises stomatal conductance and transpiration, but may still enhance evaporation at tidal saltmarsh ecosystem.

Tidal dynamics increases the nonlinearity of the controls of PAR on canopy photosynthesis and transpiration (Han et al., 2015; Guo et al., 2009). Particularly, the tidal dynamics, following the lunar cycle but not the diel solar cycle, may co-control ET with PAR, forming a complex ET pattern over the hourly and daily scales. The tides can affect ET through different paths. For instance, the tidal flooding alters physical properties of land surface (e.g., land cover, surface roughness, soil

moisture and temperature), and thus the available energy for ET. Moreover, salt marshes tend to diminish their stomata opening to deal with the stress induced by the tidal waterlogging, leading to a decrease in transpiration. Furthermore, tidal inundation may indirectly affect ET by modulating atmospheric variables such as T_a and VPD.

Because of the thermal contrast and air humidity difference between land and sea, meteorological conditions are tightly associated with wind direction (WD) in coastal regions. For instance, onshore wind tends to bring cooler and moister air from the ocean during the warm season, whereas in the cool period, it leads to higher T_a but still smaller VPD. Therefore, WD may fundamentally change the nature of the interactions between ET and the drivers in coastal ecosystems. However, the environmental controls on ET over coastal tidal saltmarsh ecosystems are yet to be investigated. This knowledge gap impedes realistic parameterizations of water and carbon flux exchange between the atmosphere and tidal ecosystems, and makes it difficult to model ET based on environmental conditions (Fisher et al., 2017).

Currently, Earth System Models (ESMs) and their embedded ET models do not explicitly consider the effects of tidal dynamics on ET, and rarely incorporate parameterizations of tidal processes for coastal ecosystems (Hurrell et al., 2013). Because of this, those models are not able to reliably and consistently capture the water and carbon exchange processes and reproduce ET in coastal areas. It is, therefore, imperative to enhance our knowledge on ET variations and drivers at coastal wetlands subject to subdaily tidal flooding.

In this study, we focus on analysing the effects of meteorological variables (i.e., PAR, T_a, VPD, WD and WS) on ET variations under tidal influence, at various timescales (from hourly to seasonal), over the coastal saltmarshes of the Yangtze Delta in the western Pacific Ocean, with the aim to improve our understanding of ET patterns and drivers at coastal wetland ecosystems imposed by tidal dynamics. The specific objectives of this paper are (1) to identify the relative importance of the environmental drivers of ET at hourly, diel, multiday, and seasonal timescales; (2) to investigate the characteristics of meteorological variables and their controls on ET under offshore and onshore wind conditions; and (3) to explore the impacts of subdaily tidal flooding on ET on the basis of 3-year EC measurements over a tidal salt marsh ecosystem of the Yangtze Delta.

2. Materials and methods

2.1. Study site description

The two sites are located in Chongming Dongtan Nature Reserve, a wetland preserve lying in the eastern part of Chongming Island in Shanghai at the mouth of the Yangtze River (Fig. 1). The Chongming Island, increasing at a rate of about 5 km² per year, is the world's largest alluvial island, and Chongming Dongtan is the fastest growing area of the island due to sediment deposition. Due to the specific scientific, economic, esthetic, and ecological values, Chongming Dongtan was accepted as an international important Ramsar site by Wetlands International Secretariat in 2002.

Chongming Dongtan is controlled by a subtropical monsoon climate, with the annual average temperature of 15.3 °C and mean annual precipitation of 1003.7 mm. It is characterized by a very hot and humid summer with a mean temperature of 26 °C and 60% rainfall during May-September, and a relatively cool and dry winter with a temperature of 3 °C on average. These climatological averages were calculated over the period 1958–1984, and released by Office of Shanghai Chronicles (2003). The land cover of Chongming Dongtan mainly consists of tidal salt marshes, tidal mudflats, and shallow open waters (Fig. 1). The predominant tidal marshes are *Phragmites australis* (common reed, hereafter *Phragmites*), *Scirpus mariqueter* (hereafter *Scirpus*), and *Spartina alterniflora* (hereafter *Spartina*) communities. *Phragmites* and *Scirpus* are native species of Chongming Dongtan, whereas *Spartina* was intentionally introduced to marshlands at
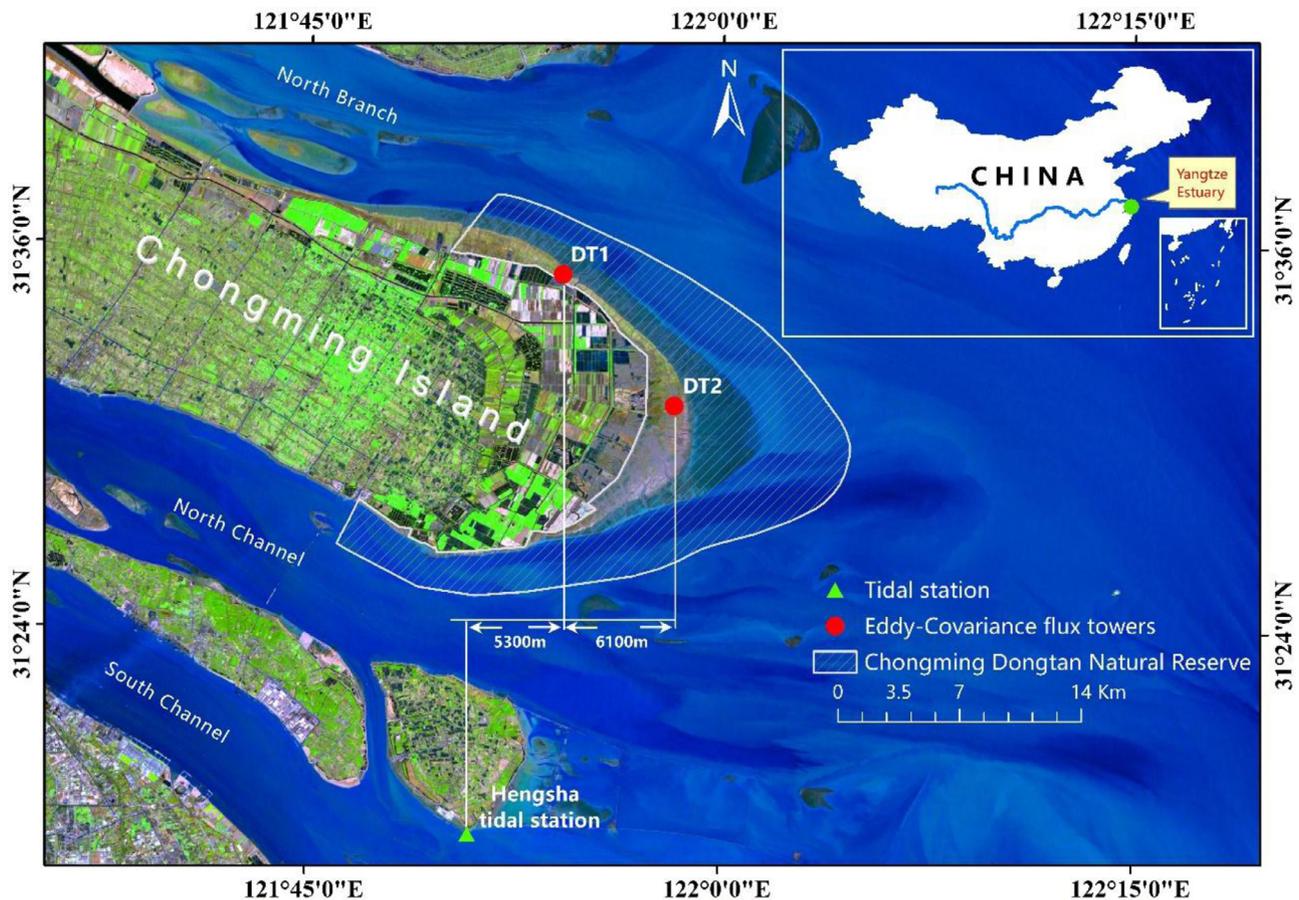
Fig. 1. Location of the two eddy-covariance flux towers (DT1 and DT2, red dots) in Chongming Dongtan Nature Reserve, and the tidal station (green triangle) in the Yangtze Estuary of China. The background is a Landsat 7 ETM + image (RGB = bands 6, 5, and 2) taken on January 01, 2007. (For interpretation of the references to color in this figure legend, the reader is referred to the web version of this article.)

Chongming Dongtan in 2001 for its strong sediment stabilization capacity (Li et al., 2009).

These two towers were established at different elevations in 2004, and have been registered in the FLUXNET database (http://fluxnet.fluxdata.org/). The inclination of the tidal flat is normally <1% (Yang et al., 2001). The EC tower (DT1) in the northern portion (31.5847°N, 121.9035°E) was located at an elevation of approximately 3.0 m above the Wusong Datum Plane, and 300 m away from the seawall (offshore) that was built in 1998. The footprint areas of the flux tower measurements were mainly within a radius of 300 m (Gu et al., 2008), and consist of *Spartina* (55%), *Phragmites* (38%), and a small portion of *Scirpus* and mudflats. Another EC tower (DT2; 31.5169°N, 121.9717°E) was also situated in the offshore side of the seawall (1600 m away) at an elevation of approximately 2.8 m. DT2 had a lower elevation and a longer distance from the seawall compared with DT1. The main flux contribution areas of DT2 were dominated by *Spartina* (72%) and *Phragmites* (25%). The percent cover of the species was estimated from the Landsat image taken on 27th November 2005 (Ge et al., 2016).

The footprint areas of DT1 and DT2 were within the elevation ranges of 3.0–3.3 m and 2.5–2.9 m (Zhao and Gao, 2018), and both featured by the semi-diurnal tides, with mean and maximum tide heights of 1.96–3.08 m (Sun et al., 2001) and 4.6–6.0 m above the Wusong Datum Plane (Yang et al., 2001). The measured tidal water level (TWL) exhibited strong semidiurnal, fortnightly and seasonal variations, as shown in Fig. 2. There were three different tidal water flooding frequencies (twice, once, and none) for the flux footprint areas in a day: (1) both the higher high water and lower high water, (2) only the higher high water, and (3) none of TWL caused tidal inundation. In

summer, the higher high water mainly happened in the nighttime, whereas the higher low water in the daytime, although the occurrence time varied (Fig. 2). Spring tides tended to induce flooding both in the daytime and nighttime, whereas during neap tides, no tidal inundation occurred. The flux contribution areas of DT2 were to a greater degree inundated by tidal seawater relative to DT1, since it was located in a lower elevation.

2.2. Flux tower and tidal water

In this study, we used the flux data as well as meteorological parameters during the period 2005–2007 that were measured by two EC towers in the Chongming Dongtan wetland (Fig. 1). The open-path EC systems were used to measure momentum, heat, H_2O and CO_2 fluxes, as well as additional biological and meteorological parameters, including net radiation (R_n), PAR, rainfall, relative humidity (RH), T_a, VPD, soil water content, soil temperature (T_s), WD, and WS.

Sensible heat fluxes (H) and LE were measured by the EC method with a three-axis sonic anemometer (CSAT-3, Campbell Scientific Inc., Logan, UT, USA) and open path infrared gas analyser (IRGA, Li 7500, LI-COR Inc., Lincoln, NE, USA) positioned at the height of 4.8 m above the surface. Soil heat fluxes (G) were measured by Radiation Energy Balance Systems (HFT-3, Campbell Scientific Inc., USA) at the depth of 0.05 m.

A net radiometer (CNR1, Kipp and Zonen, Delft, Holland) was used to measure net radiation (R_n) above the canopy (2 m). The LI-190SZ Quantum Sensor and the LI200SZ Pyrometer Sensor (LI-COR, Inc., USA) were used to measure PAR and photosynthetic photon flux density (PPFD), respectively. Rainfall was measured with a tipping bucket rain
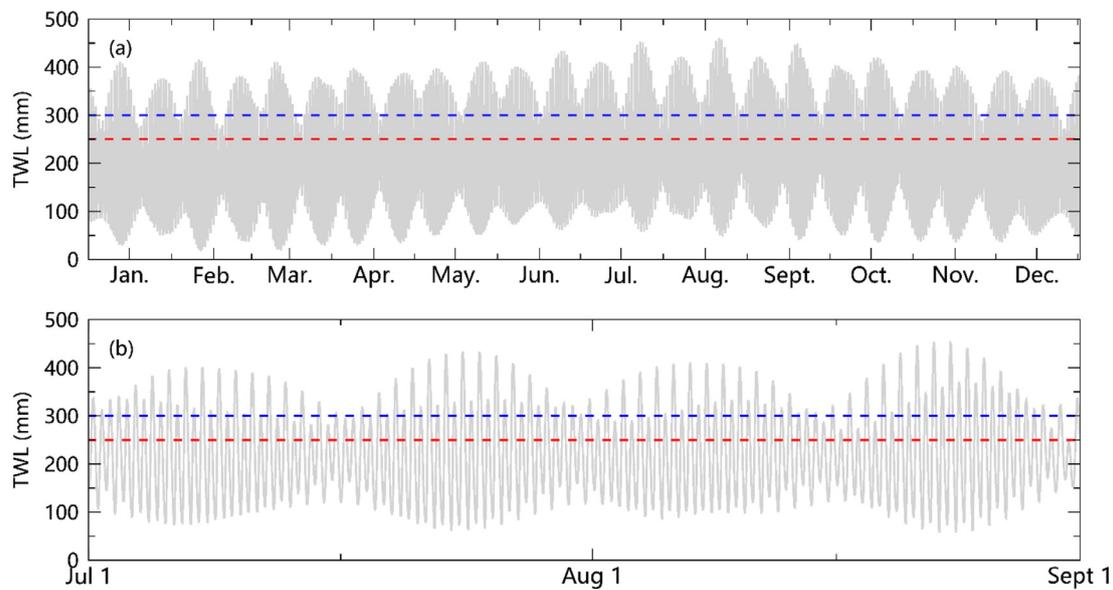
Fig. 2. Variations of tidal water level (TWL) above the Wusong Datum Plane measured by the Hengsha tidal station during the periods (a) January 1–December 31 and (b) July 1–August 31 of 2005. The blue and red dashed lines represent the lowest elevations of the footprint areas of DT1 and DT2, respectively. (For interpretation of the references to color in this figure legend, the reader is referred to the web version of this article.)

gauge (TE525, Texas Electronics, Texas, USA) mounted 4.6 m above the ground. RH and T_a were observed using shielded sensors (HMP-45, Vaisala Helsinki, Finland). A reflectometry sensor (CS616, CSI) and soil moisture sensors (model 257, CSI) were used to measure soil temperature and moisture at the depth of 0.05 m at each site, respectively.

We obtained the TWL during the period 2005–2007, which were recorded at one-hour interval by the nearest tidal station HengSha (Fig. 1), and have been interpolated to half-hourly data for a better comparison with the EC measurements.

2.3. Quality control and gap filling

With consideration of the impacts of water vapour on the sonic temperature measurements, air density, and equipment malfunction, several corrections were made before calculating the turbulent fluxes. More specifically, we rotated the wind velocity to make the 0.5 hourly mean vertical and cross-wind components equate to 0. The effect of water vapour on the sonic temperature measurements was limited following Kaimal and Gaynor (1991). High-frequency loss of signals resulting from equipment malfunction were corrected as Moore (1986). Moreover, the effect of air density fluctuation on heat fluxes has been rectified according to Webb et al. (1980).

All measured EC flux data have been checked for their quality, and the quality control was processed with EdiRe data software, which was developed by School of Geosciences, the University of Edinburgh, England (Clement, 1999). The stationary tests were applied following Foken and Wichura (1996), with the rejection threshold set to 30%. In addition, the integral turbulence test was performed for σ_w/u_* as suggested by Kaimal and Finnigan (1994), where σ_w represents the 0.5 hourly standard deviation of vertical WS, u_* is the friction velocity. As a result of the quality control, about 19.8% and 24.8% of the data were rejected for DT1 and DT2, respectively.

The gaps of the half-hourly EC data due to unfavourable micrometeorological conditions or instrument failure were filled by using the online tool (http://www.bgc-jena.mpg.de/~MDIwork/eddyproc/) offered by the Max Planck institute for Biogeochemistry (MPI-BGC), based on the method proposed by Reichstein et al. (2005).

2.4. Flux footprint analysis and energy balance closure

We used the two-dimensional parameterization for flux footprint prediction (Kljun et al., 2015), which is an improved version of the footprint model of Kljun et al. (2004). This parameterization not only offers the extent but also the width and shape of footprint estimates. Moreover, it considers the effects of the surface roughness length explicitly. The inputs of the model are measurement height above the displacement height, mean WS, boundary layer height, Obukhov length, standard deviation of lateral velocity fluctuation, and friction velocity. In this study, the displacement height is estimated as 0.67 times the height of the canopy at two sites.

In general, the energy balance equation at the surface can be written as:

$$R_n - G = H + LE + \Delta , \tag{1}$$

where R_n is the net radiation [W m^{-2}], H the sensible heat flux [W m^{-2}], LE the latent heat flux [W m^{-2}], G the ground heat flux [W m^{-2}], and Δ the residual heat [W m^{-2}] due to measurement error or missing terms. In coastal wetlands, Δ is associated with the heat energy flow with tidal water (Moffett et al., 2010).

ET was inferred from the EC derived LE divided by the latent heat of vaporization for water ($\lambda = 2.45$ MJ kg^{-1}). Strictly speaking, λ is not a constant because it is related to atmospheric pressure and temperature, but 2.45 MJ kg^{-1} is widely accepted for the calculation.

The energy balance closure was evaluated for each site-year using the energy balance ratio (EBR) (Mahrt, 1998), which was calculated by the following equation over a period of one year. It is noted that the data excludes those in rainy days and nocturnal conditions when u_* was less than 0.15 m s^{-1} (Chen et al., 2009).

$$EBR = \frac{\sum (H + LE)}{\sum (R_n - G)}, \tag{2}$$

2.5. Eco-atmosphere interaction analysis

The information theory was used to characterize the eco-atmosphere interactions. The mutual information (I) describes the averaged tendency for paired states of two variables (X and Y) to coexist (Fraser and Swinney, 1986), while the relative mutual information (IR
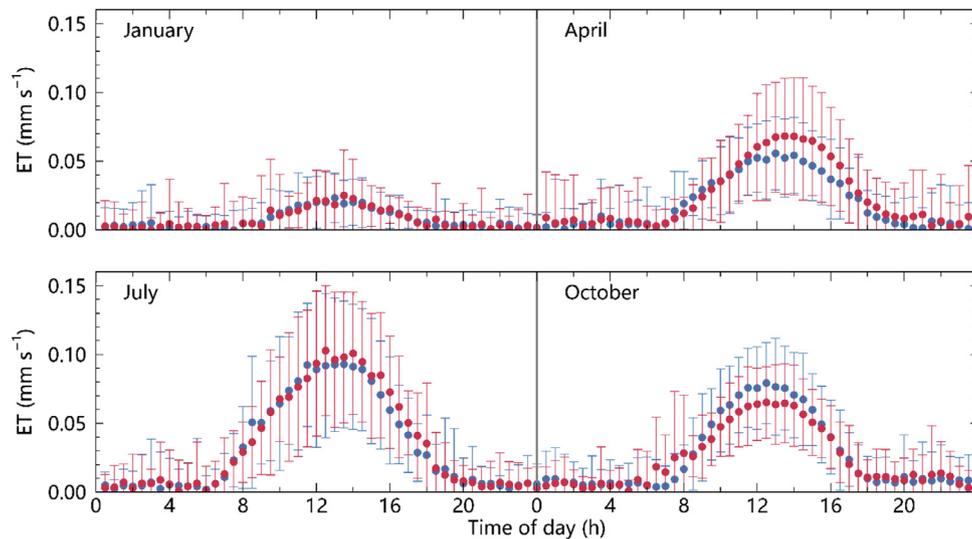
Fig. 3. Averaged diel patterns of ET for the two coastal wetland sites DT1 (blue circles) and DT2 (red circles) in January, April, July, and October of 2005–2007. The bars stand for standard deviations. (For interpretation of the references to color in this figure legend, the reader is referred to the web version of this article.)

or $IR_{X,Y}$) represents the proportion of bits needed to represent Y that are redundant given the knowledge of X. IR reflects not only the similarity in the shape of pattern but also in the magnitude of variability, and is able to identify both linear and nonlinear interactions. Moreover, the statistical strength and the asynchrony of the eco-atmosphere interaction can also be detected. If the maximum IR is found at zero time lag ($\tau = 0$), the interaction is characterized as 'synchronous'. Otherwise, the interaction is identified as 'asynchronous', namely variations in Y lagged (maximum $IR_{X,Y}$ at $\tau > 0$) or lead (maximum $IR_{X,Y}$ at $\tau < 0$) variations in X (Knox et al., 2018; Sturtevant et al., 2016).

The analysis was conducted to characterize the interactions between ET and the drivers at the hourly, diel, multiday, and seasonal timescales during the period 2005–2007. Apart from TWL, PAR, VPD, T_a, T_s, u_*, WS, and WD were also included in the analysis, as they were theoretically connected with ET variations (Monteith and Unsworth, 2013). The procedure was implemented in our study as follows. First, the maximal overlap discrete wavelet transform (MODWT) was applied to decompose the data into the hourly (scales 1–2, 1–2 h), diel (scales 3–6, 4 h to 1.3 days), multiday (scales 7–10, 2.7–21.3 days), and seasonal (scales 11–14, 42.7–341 days) timescales based on the WMTSA wavelet Toolkit in Matlab (Cornish et al., 2006). The next step is to use the ProcessNetwork software version 1.5 (Ruddell et al., 2008) to compute IR between ET and environmental variables at each timescale. The maximum evaluated lags were respectively set up to 0.5, 1, 5, and 100 days at the hourly, diel, multiday, and seasonal timescales, and a Monte Carlo approach was used to estimate statistical significance at the 95% level, following Sturtevant et al. (2016).

Furthermore, we applied the same procedure to compute the IR between ET and environmental variables during the daytime and nighttime at the four timescales, in order to distinguish the extents to which the environmental variables exerted controls on ET between day and night. The data during the hours 6:00–18:00 (local time) were used to characterize the eco-atmosphere interactions in the daytime, while the other data were for the analysis in the nighttime, since sunrise usually occurs during 5:00–7:00 and sunset during 17:00–19:00 for the whole year in the study area that is located in the latitude of 31°N.

2.6. Investigating the response of ET to wind direction and tidal inundation

With the aim to examine the effect of the air mass condition that is characterized with wind direction on ET at coastal saltmarsh, we plotted the averaged diel variation of ET and its tightly associated meteorological variables (i.e., PAR, VPD, T_a, and WS) under onshore

(easterly, 45–135°) and offshore (westerly, 225–315°) wind conditions in May-October (warm period) and November–April (cool period), respectively. Moreover, the responses of ET to PAR, VPD, T_a, and WS during 10:00–15:00 h in warm periods were also investigated on a half-hourly basis, and their relationships were tested by fitting linear, polynomial, exponential, and power equations to the data. In addition, the information theory approach was applied to characterize the interactions between ET and the environmental variables under offshore and onshore wind conditions, in order to address the role that wind direction played in structuring the environmental drivers.

To investigate the effect of tidal inundation on ET, we calculated the averaged diel variations of ET, PAR, VPD and T_a at both sites when TWL was, respectively, greater than 3.0, 2.5 m and lower than 2.0, 1.5 m for DT1, DT2 under offshore (225–315°) and onshore (45–135°) wind condition based on EC data during May–October of 2005–2007. We selected the TWL of 3.0 and 2.5 m as the lower boundary for high tides, and 2.0 and 1.5 m as the upper boundary for low tides, due to the elevations of the footprint areas. It is estimated that the footprint areas of DT1 and DT2 were inundated by seawater when the TWL was higher than 3.0 and 2.5 m, whereas when TWL was less than 2.0 and 1.5 m, their footprint areas were mostly not flooded (Fig. 2). Furthermore, we studied the responses of ET to PAR, VPD, T_a, and WS during 10:00–15:00 h at low and high tides, on a half-hourly basis, under different wind conditions in warm periods, and their relationships were tested by fitting linear, polynomial, exponential, and power equations to the data.

3. Results

3.1. Diel patterns of ET and meteorological variables

Fig. 3 shows the mean diel patterns of ET for the two coastal wetland sites (DT1 and DT2) in January, April, July, and October of 2005–2007, respectively. ET peaked between 11.5 h (local standard time) and 12.5 h with peak values of 0.023, 0.056, 0.093 and 0.079 mm s^{-1} for DT1, and 0.025, 0.068, 0.103 and 0.065 mm s^{-1} for DT2 in January, April, July and October, respectively. ET reached the peak approximately 0.5–1.5 h later than PAR, whereas 1–1.5 h earlier than T_a. The diurnal peak of VPD generally occurred later than that of ET, but sometimes slightly earlier than T_a (Fig. S1).

The magnitudes of the diel variation in ET were largest in July, followed by October, and lastly by January, whereas that in PAR were largest in April, followed by July, and lastly by January. On the other
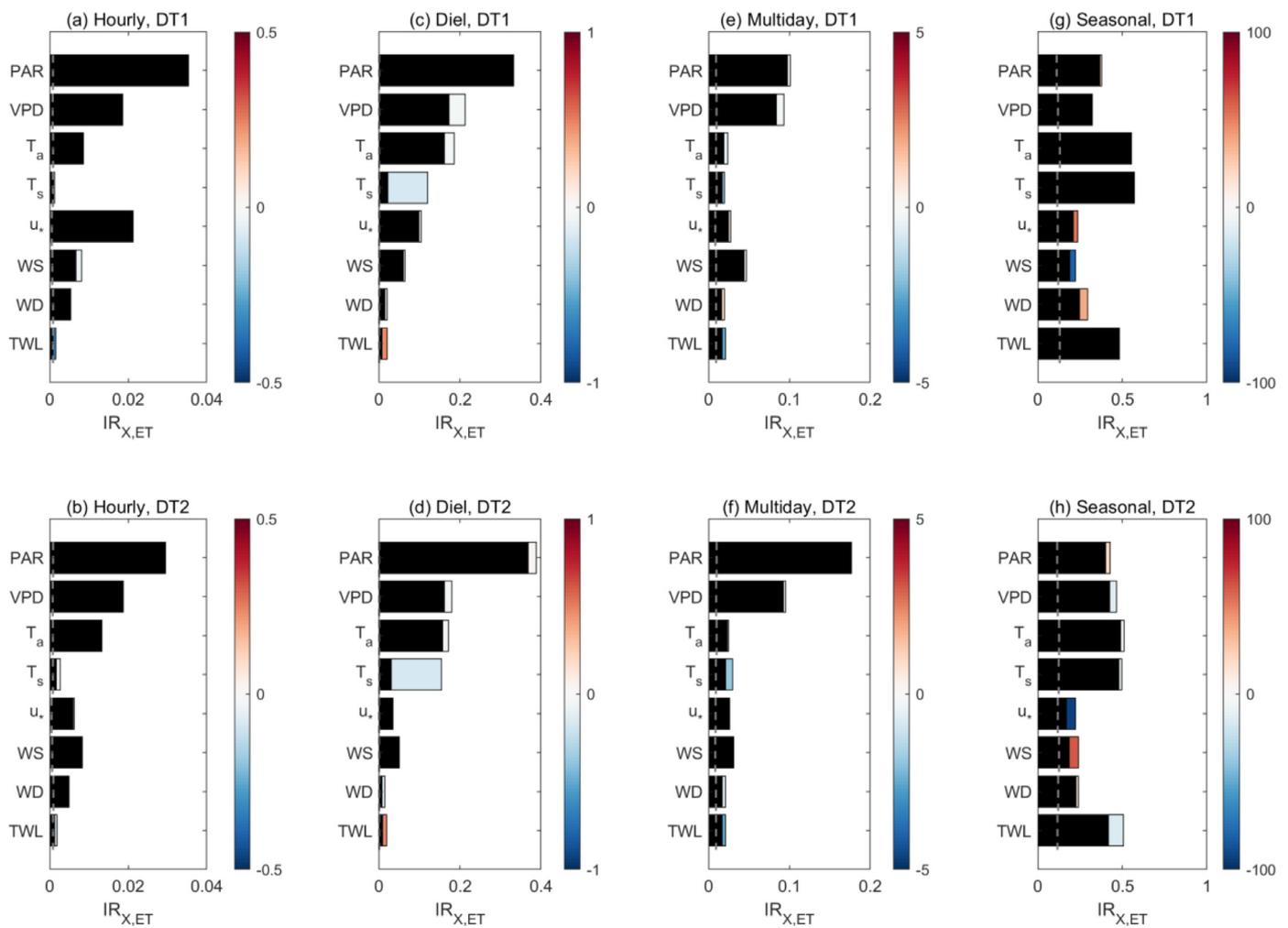
Fig. 4. Relative mutual information ($IR_{X,ET}$) between ET and the potential drivers at (a, b) hourly, (c, d) diel, (e, f) multiday, and (g, h) seasonal timescales for DT1 and DT2. The subscript x represents each variable on the y axis. The length of each black bar represents IR without any time lag, whereas the coloured extension indicates the maximum IR and the colour shows whether the process involves a lead or lag. Red (blue) shows that variability in ET lagged (led) the variability in environmental variables. The colour bar units are in days, and the vertical grey lines indicate the 95% significance threshold. (For interpretation of the references to color in this figure legend, the reader is referred to the web version of this article.)

hand, it appears that T_a and VPD corresponded well with the magnitudes of diel variability of ET (Fig. S1). This suggests that, over the season, the magnitude of diel ET variations is determined more by T_a and VPD rather than PAR.

### 3.2. Multiscale interaction between ET and environmental variables

ET shared the largest mutual information with PAR, followed by VPD, and their interaction processes were highly or nearly synchronous at the hourly, diel, and multiday timescales at both sites (Fig. 4). More specifically, the maximum $IR_{PAR, ET}$ were 0.33, 0.10 and 0.38 at DT1, and 0.39, 0.18 and 0.43 at DT2, whereas the values between VPD and ET were 0.02, 0.21 and 0.09 at DT1, and 0.02, 0.18 and 0.10 at DT2 at diel, multiday, and seasonal scales, respectively. This indicates that, consistently, PAR was the most important driver for ET variability, and VPD was the second major control at the three timescales. At the diel scale, T_a and T_s also appeared to play important roles. In contrast, at the seasonal scale, TWL, T_a, and T_s exerted dominant effects on ET variability, while PAR became a less important driver.

In general, the values of IR were comparatively high at the seasonal scale (in the range of 0.2–0.5), whereas low at the hourly scale (<0.04), which are indicated by the different IR ranges in Fig. 4. This illustrates that, generally, the interaction strengths between ET and

environmental variables were strongest at the seasonal scale, followed by the diel scale, while the weakest interactions occurred at the hourly scale. This result is not surprising because the measurement uncertainty tends to be large at the hourly scale (Hollinger and Richardson, 2005).

The maximum $IR_{TWL, ET}$ were 0.002, 0.02, and 0.02 for both sites at the hourly, diel, and multiday scales, whereas at the seasonal scales, the values were respectively 0.48 and 0.51 for DT1 and DT2 (Fig. 4). Although the IR were rather small from diel to seasonal timescales, there were significant linkages between ET and TWL at the three timescales for both sites ($p < 0.05$). The seasonal scale showed the highest interaction strength between ET and TWL, as indicated by the $IR_{TWL, ET}$ of 0.48 and 0.51 for DT1 and DT2. TWL appeared in advance of ET by approximately 11.5 h for both sites at the diel scale, whereas at the multiday and seasonal scales, TWL lagged ET by up to 2.40 and 2.60 days for DT1, and 2.44 and 15.65 days for DT2, respectively. This corresponds with the semidiurnal, spring-neap, and annual tidal cycles in the study area, suggesting that the tidal dynamics exerted rather strong effects on ET variations. It is noted that the main drivers for the ET variations were rather similar at various timescales, but the extents to which they controlled ET were different, which will be discussed later.

We found that in Fig. 5, from hourly to multiday timescales, ET had the strongest interactions with PAR and VPD in the daytime, whereas
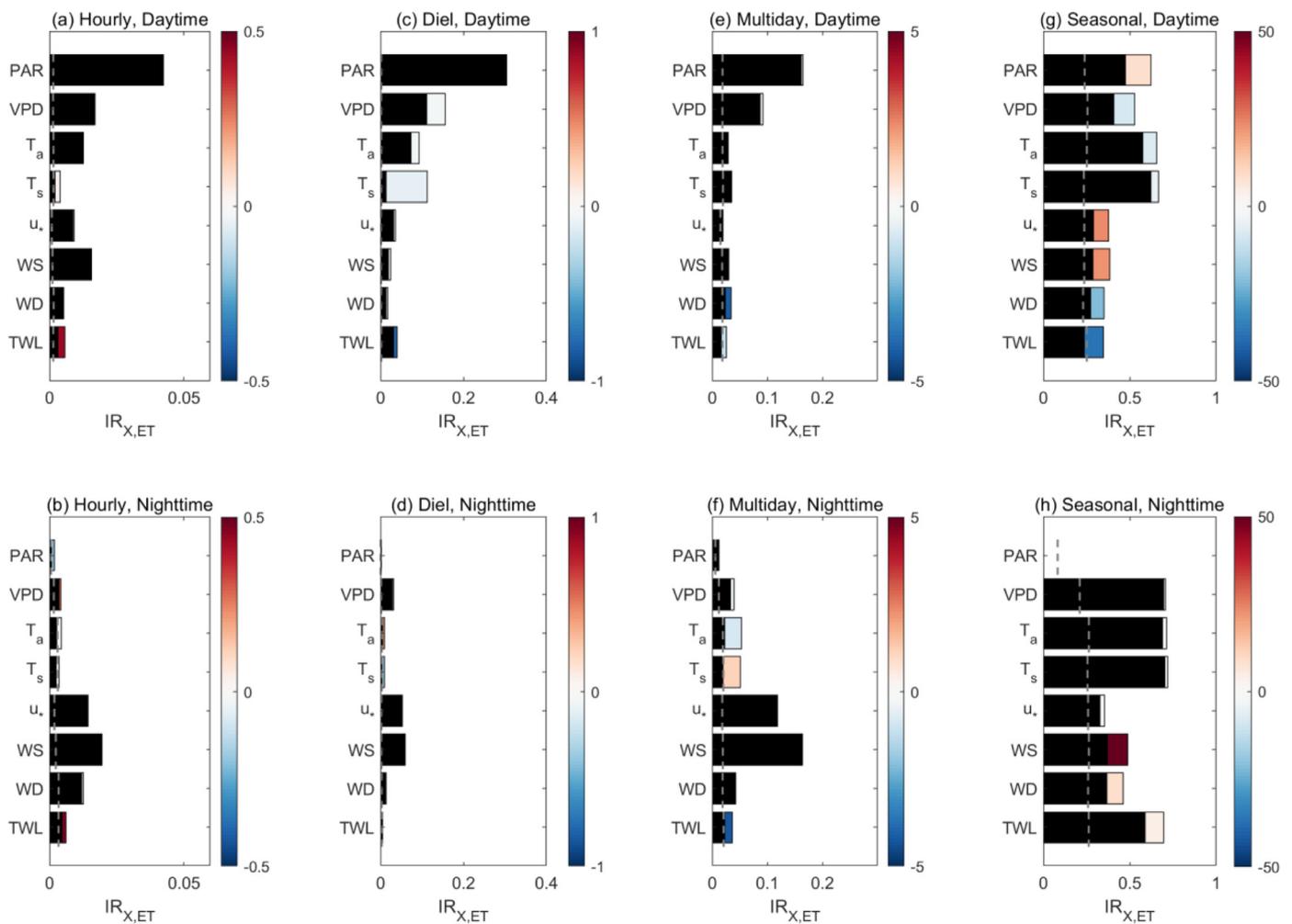
Fig. 5. Relative mutual information ($IR_{X,ET}$) between ET and the potential drivers at (a, b) hourly, (c, d) diel, (e, f) multiday, and (g, h) seasonal timescales in the daytime (local time 6:00–18:00) and nighttime (local time 18:00–6:00) for DT1. The subscript x represents each variable on the y axis. The length of each black bar represents IR without any time lag, whereas the coloured extension indicates the maximum IR and the colour shows whether the process involves a lead or lag. Red (blue) shows that variability in ET lagged (led) the variability in environmental variables. The colour bar units are in days, and the vertical grey lines indicate the 95% significance threshold. (For interpretation of the references to color in this figure legend, the reader is referred to the web version of this article.)

during the nighttime, WS and u_* played dominant roles in ET variability. More specifically, the maximum $IR_{PAR, ET}$ at DT1 were 0.04, 0.30, and 0.16 during daytime at the hourly, diel, and multiday scales, whereas the values were very small, which was consistent with the fact that PAR was only available in the day. The maximum $IR_{VPD, ET}$ were 0.02, 0.16, and 0.10 during the day at the three timescales, which were 3.25, 4.02, and 1.36 times higher than that during the night. Although WS and u_* had near-synchronous and significant interactions with ET during both the day and night, the $IR_{WS, ET}$, $IR_{u*, ET}$ in the nighttime were 0.06, 0.05 at the diel scale, and 0.16, 0.12 at the multiday scales, which were respectively 1.7, 3.0 and 6.0, 5.3 times that in the daytime. At the seasonal scale, T_a and T_s had the strongest interactions with ET, with the IR values higher than 0.5, during both daytime and nighttime. TWL appeared to have stronger interaction with ET in the night.

### 3.3. Response of ET to wind direction

Fig. 6 shows that, when wind direction changes, the magnitudes of diel variations of ET and major meteorological variables, namely PAR, T_a, VPD and WS, are distinct. In warm periods, the mean daytime ET peak increased from 0.07 mm s^{-1} under offshore wind to 0.10 mm s^{-1} under onshore wind (Fig. 6b). The ET pattern was strongly correlated to PAR, the peak of which rose from 700 μmol m^{-2} s^{-1} under offshore wind to 1000 μmol m^{-2} s^{-1} under onshore wind with a similar time

(Fig. 6c). On the other hand, offshore wind created larger difference of T_a, VPD, and WS between day and night in both warm and cool periods.

Generally, the values of IR between ET and meteorological variables were higher under offshore wind conditions than that under onshore wind conditions at different time scales for both sites (Fig. 7). The differences were especially pronounced at the multiday scales, as the values of IR between ET and PAR, VPD, T_a, and T_s were greater than 0.4 when offshore wind prevailed, whereas under onshore wind conditions, they were mostly smaller than 0.2. PAR had the largest mutual information with ET under both wind conditions, and did not change much when the wind shifted direction at the hourly and diel scales, whereas at the multiday scales, VPD, T_a, and T_s played an equal role as PAR in ET variations.

The multiday scale showed more significant interactions between ET and TWL when the wind was blowing offshore, as illustrated by the fact that $IR_{TWL, ET}$ under offshore wind were 0.21 and 0.15, whereas under onshore wind condition, the values were 0.06 and 0.07 for the two sites. This indicates that tidal effects on ET were more pronounced when offshore wind prevailed.

The half-hourly data during 10:00–15:00 h exhibited that ET had significant relationships with PAR (exponential, $R^2 = 0.62$), VPD (linear, $R^2 = 0.55$), T_a (power, $R^2 = 0.35$), and WS (linear, $R^2 = 0.25$) when offshore wind prevailed, whereas under onshore wind condition, ET had no significant correlations with VPD, T_a, and WS (Figure S2),
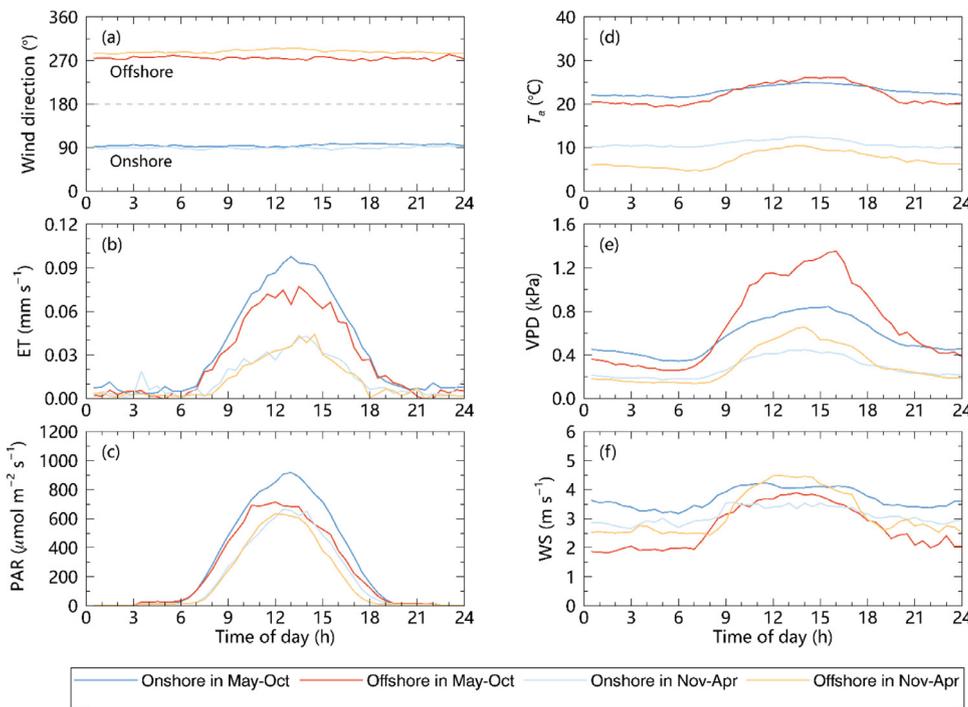
Fig. 6. Averaged diel variations of EC tower measured (b) ET, (c) PAR, (d) T_a, (e) VPD, and (f) WS under (a) onshore (45–135°) and offshore (225–315°) wind conditions during May–October (warm period) and November–April (cool period) from 2005 to 2007 at DT2. (For interpretation of the references to color in this figure legend, the reader is referred to the web version of this article.)

which was consistent with the fact that PAR was the dominant driver on ET variation during the daytime regardless of wind condition at the hourly and diel scales (Fig. 7).

3.4. Response of ET to tidal inundation

The major difference of daytime ET, PAR, VPD and T_a between high and low TWL occurred under offshore wind condition, suggesting that tidal inundation exerted notable effects on diel variations of ET during May-October. On the other hand, when the wind was blowing onshore, the diel variations of ET, PAR, VPD and T_a were comparable during flooded and non-flooded conditions. More specifically, when an offshore wind prevailed, the mean diel variations of ET during high tides were up to 0.07 mm s^{-1} higher than that during low tides for the two sites in the daytime (Fig. 8 (a, e)). Similarly, the daytime PAR under high TWL, to the greatest extent, increased by 256.1 and 496.2 µmol m^{-2} s^{-1} respectively for DT1 and DT2, compared with that under low TWL (Fig. 8 (b, f)). Moreover, tidal submergence appeared to reduce T_a by up to 5.6, 8.5 °C, and VPD by 0.9, 1.2 kPa at the two sites, as observed in Fig. 8 (c, g) and (d, h).

In general, ET exhibited stronger relationships (with higher R^2) with the meteorological variables during low tides than that with high tides (Figure S3). ET responded to PAR with rather similar sensitivities under both tidal conditions. However, the sensitivities of ET to VPD, T_a and WS differed when TWL was high. The tidal inundation appeared to increase and suppress the sensitivities of ET in response to VPD and WS, respectively.

4. Discussion

#### 4.1. Tidal effects on ET and the mechanism

As with most terrestrial ecosystems, PAR is a major control on ET at hourly, diel and multiday timescales in the coastal saltmarsh ecosystem, indicated by the strongest linkages between ET and PAR (Fig. 4). VPD, T_a, T_s, u_*, and WS are also important drivers for ET variability in coastal wetlands at various timescales. However, different from upland ecosystems, the tide is an important factor influencing the ET process in the coastal wetland, reflected by the significant relationship ($p < 0.05$)

between TWL and ET from hourly to seasonal timescales (Fig. 4).

In the warm season, midday tidal flooding directly transferred the salt marsh to a cool and wet surface, in contrast to its warm-surface characteristics under non-inundation conditions, leading to a change on surface energy partitioning and thus ET. During midday in the warm season, the cool tidal waters led to a 3.0% reduction on average in the surface-emitted longwave radiation at DT1 (Table 1). There were 17.3% and 29.4% decreases in H and G during flooding compared to non-flooded condition (Table 1), which was partly attributed to the fact that the cooler tidal water decreased or reversed the temperature gradient between salt marsh-air and salt marsh-top soil. In addition, the residual heat in the midday was 16.2 and −6.9 W m^{-2} on average during flooded and non-flooded conditions, implying that the cool tidal waters absorbed heat from the atmosphere.

The altered heat exchange at salt marsh-atmosphere interface during tidal inundation was associated with the increased aerodynamic resistance, as the flooding decreased roughness of the mudflat and salt marshes in the flux footprint area, which was reflected by the lower u_* compared to non-flooded conditions (Table 1). This can also explain the reason why the sensitivity of ET in response to VPD increased, but decreased in response to WS when the wetland was inundated. Although R_n was smaller, the 23% reduction in LE that is directly linked to ET during flooding was due to, on the one hand, the decrease in H and G, and on the other hand, the heat absorption of tidal waters. Apart from available energy, tidal submergence may result in soil hypoxia or anoxia, and consequently decrease overall plant metabolic activity and diminish stomatal opening, leading to transpiration cessation (Banach et al., 2009; Kathilankal et al., 2011; Moffett et al., 2010).

Tidal inundation both occurred in the daytime and nighttime in the study area. However, plant transpiration, soil and plant evaporation all contributed to ET dramatically during the daytime, whereas during the nighttime, evaporation is the main contributor to ET since vegetation transpiration is rather small without solar radiation. This explains the reason why, during the night, WS and u_* imposed dominant controls on ET at hourly, diel, and multiday scales, as shown in Fig. 5. The tides appeared to exert stronger effects on ET during the nighttime, at the multiday and seasonal scales, in comparison with daytime, because PAR, the main ET driver in the daytime, was typically not influenced by the tides. Moreover, the occurrence frequency and duration of the tidal
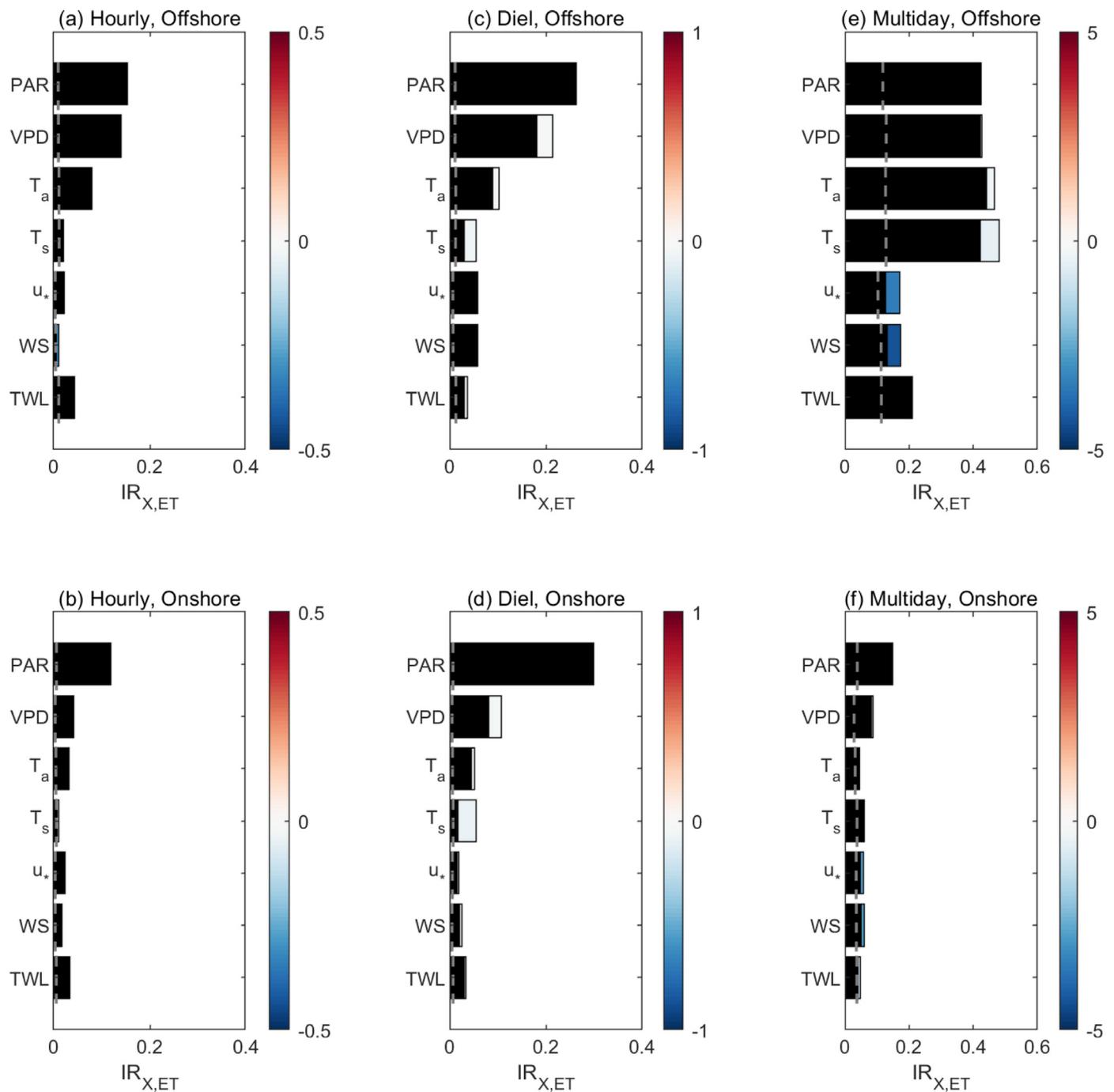
Fig. 7. Relative mutual information ($IR_{X, ET}$) between ET and the potential drivers under (a, c, e) offshore and (b, d, f) onshore wind conditions at (a, b) hourly, (c, d) diel, and (e, f) multiday timescales in the daytime (local time 6:00–18:00) for DT1. The subscript x represents each variable on the y axis. The length of each black bar represents IR without any time lag, whereas the colored extension indicates the maximum IR and the colour show whether the process involves a lead or lag. Red (blue) shows that variability in ET lagged (led) the variability in environmental variables. The colour bar units are in days, and the vertical grey lines indicate the 95% significance threshold. (For interpretation of the references to colour in this figure legend, the reader is referred to the web version of this article.)

inundation in the night were larger than that during the day (Fig. 2).

In the coastal wetland, wind direction fundamentally changed the nature of the interactions of ET with other variables (Fig. 7), due primarily to the thermal contrast and air humidity difference between land and sea. Onshore wind brought cool air from the Pacific Ocean during the warm season, whereas it transported heat to the coastal salt marshes in the cool periods. In contrast, offshore wind lifted up T_a in the warm period, while cooled it down in the cool period. This led to the result that, during the warm periods, the mean daytime T_a under offshore air mass was higher than onshore air mass, while the contrary was the case

in the cool periods, as shown in Fig. 6d. Moreover, the offshore air mass was transported from the inland with less moisture all year round, and hence resulting in higher levels of VPD (Figs. 6e and S2 (b, f)) in comparison with onshore air mass.

Tidal flooding appears to impose a limited impact on daytime PAR, T_a, VPD, and ET when wind was blowing onshore in May-October, which is very much different from that under offshore wind condition (Fig. 7). The reasons for this can be explained as follows. Onshore wind from the ocean brought relatively wet and cool air mass during May-October, and thus resulted in low levels of VPD and T_a, which was
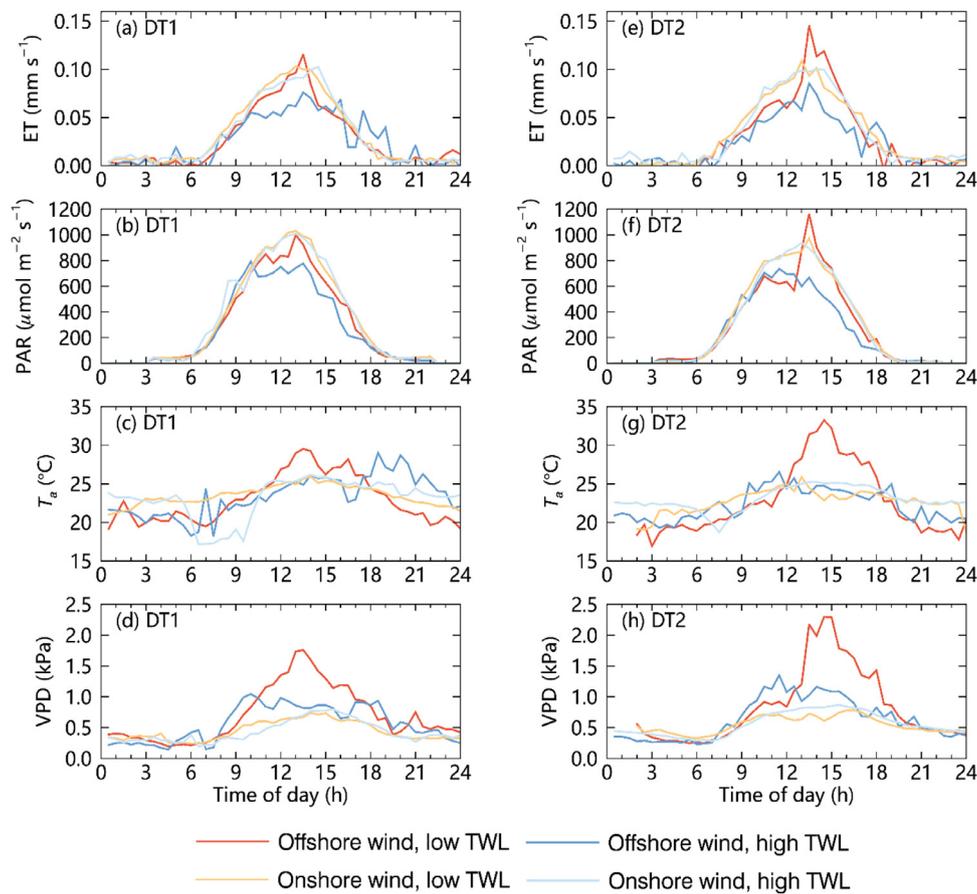
Fig. 8. Diel variations of (a, e) ET, (b, f) PAR, (c, g) T_a, and (d, h) VPD when TWL was lower than 2.0 and 1.5 m (low TWL), and higher than 3.0 and 2.5 m (high TWL) at DT1 and DT2, respectively, under offshore (225–315°) and onshore (45–135°) wind conditions during May–October of 2005–2007.

Table 1

Comparison between net radiation (R_n), latent heat flux (LE), sensible heat flux (H), ground heat flux (G), outgoing longwave radiation (R_{glout}), residual heat (Δ), and friction velocity (u_*) at high and low TWLs in the midday (10:00–15:00) during May-October of 2005–2007 at DT1. Units for the energy budget components and u_*: W m^{-2} and m s^{-1}. Note: Δ was estimated from Eq. (1).

	High TWL	Low TWL	+/-	+/− (%)
R_n	334.0 ± 119.4	363.4 ± 158.0	− 29.4	− 8.1%
LE	145.4 ± 38.8	190.0 ± 25.8	− 44.6	− 23.5%
H	107.4 ± 43.4	129.8 ± 45.4	− 22.4	− 17.3%
G	16.8 ± 16.6	23.8 ± 18.0	− 7.0	− 29.4%
R_{glout}	455.3 ± 8.3	469.3 ± 10.0	− 14.0	− 3.0%
Δ	16.2 ± 70.9	− 6.9 ± 76.2	23.1	334.8%
u_*	0.49 ± 0.067	0.47 ± 0.065	0.02	4.3%

rather similar with the effects of tidal flooding. As a result, the effect of tidal inundation on ET was not pronounced under the onshore wind condition.

Tidal inundation exerted indirect effects on ET through modulating meteorological variables over the salt marsh ecosystem, which can be confirmed by the distinct features of averaged diel variations of PAR, VPD, T_a, and WS, and different sensitivities of ET in response to the meteorological variables under high and low TWLs when the wind was blowing offshore (Fig. S3). Flooding notably suppressed daytime VPD and T_a, leading to a decrease in ET at both sites.

4.2. Comparison between the two sites

There were some apparent differences between the two coastal

wetland sites, although they exhibited similar patterns of temporal variations in ET and the meteorological controls. First of all, the magnitudes of diel variations of ET were different between the two sites (Fig. 3). The ET of DT2 in the midday (10:00–15:00) was on average 20.9% higher with 26.1% larger dispersion than that of DT1 in April, whereas in October, the ET of DT2 was 13.3% lower in value with 11.4% less variation than that of DT1. The difference of ET in April was mainly due to the fact that, relative to DT2, DT1 had larger temperature gradients between upper soil and air (lower T_s but higher T_a) in the midday (Figure S1), which induced significantly more G to warm the soil and more H to heat the atmosphere (Figure S4), and consequently less heat energy for ET. In October, T_s and T_a of DT1 were slightly lower than that of DT2 in the midday, though to a different extent, leading to little difference in G and more energy available for H and LE. The other reason may be that DT1 had greater canopy transpiration due to higher PAR and lower VPD in comparison with DT2 (Fig. S1).

Second, the extents to which the meteorological variables control ET were different between the two sites. The maximum $IR_{PAR, ET}$ of DT2 were 18.2%, 80.0%, and 13.2% higher than that of DT1 at diel, multiday, and seasonal scales, respectively (Section 3.2). This may be because, relative to DT1, tidal flooding occurred more frequently and lasted longer at DT2, and had more influence on the meteorological variables such as VPD and T_a, but PAR was not directly linked to the tides. For similar reasons, u_* and WS shared larger mutual information with ET at DT1 compared with DT2, especially at the hourly and diel timescales (Fig. 4). Since the mean and peak flow speeds were about 1.0 m/s and 2.0 m/s (GSCCI, 1988), it was estimated that the tidal currents spent about 0.84–1.69 h to move between DT1 and DT2 (the distance between the sites 6100 m, as shown in Fig. 1, divided by the flow speeds). This corresponded with the fact that the difference

between the time lags of the maximum $IR_{TWL, ET}$ of two sites was 1.0 h at diel scale (Section 3.2).

Third, the degrees of energy balance closure at the two sites differed to a certain extent. The values of EBR of DT1 ranged from 0.91 to 0.96 during 2005–2007, which was consistently higher than that of DT2 in the range between 0.71 and 0.78 (Table S1). This can be attributed to the fact that the spatial heterogeneity of DT2 was greater than that of DT1 (Fig. S5), which resulted in stronger advection of scalars (Wilson et al., 2002). Moreover, DT1 appeared to have a greater degree of instability of the atmosphere in comparison with DT2, as indicated by higher H (Fig. S4), leading to an improvement of the energy balance closure (Monteith and Unsworth, 2013). The tide may also be one of the main contributors to the different extent of surface energy imbalance at the two sites, since in coastal ecosystems, the storage terms that are subject to tidal export contributed to the non-closure of the surface energy balance (Malone et al., 2014).

The maximum length of the flux footprint under onshore and offshore wind conditions reached roughly 400 m (Fig. S5). This was smaller than the empirical fetch length (480 m) calculated by using the measurement height (4.8 m) multiplied by 100 (Nicolini et al., 2017), demonstrating that the two EC towers were able to reliably measure water and heat fluxes between salt marsh-atmosphere. Despite the existence of surface energy imbalance, the values of EBR ranging from 0.71 to 0.96 illustrated that our data at two sites have good quality, since non-closure of the surface energy balance is often present due to instrument biases, advection and neglected energy sinks such as canopy heat storage and metabolic terms (Stoy et al., 2013; Wilson et al., 2002).

5. Conclusions

Understanding ET pattern and its drivers at coastal wetlands imposed by subdaily tidal flooding helps to bridge the gap between ET processes in coastal and inland ecosystems, and enhance our knowledge in global water and energy cycles. In this study, we investigated the meteorological controls on ET at coastal wetlands under lunar semidiurnal tidal influence, on the basis of EC measurements over a tidal salt marsh ecosystem in the Yangtze Delta during 2005–2007. We found that ET variations were mainly controlled by PAR from hourly to multiday scales at the coastal salt marsh ecosystem, whereas over the season, T_a, T_s, and VPD played a more important role in ET variation than PAR. During the daytime, ET was primarily driven by PAR and VPD, whereas during the nighttime, WS and u_* dominated the variability of ET.

The tidal dynamics complicated the controls of meteorological factors, namely PAR, T_a, and VPD, on ET processes, forming a complex ET pattern at the hourly and subdaily scales. This is due to the fact that the tides and PAR are driven by different objects, the sun and the moon respectively, and tidal flooding occurs in different phases of solar day. TWL exerted stronger effects on ET during the nighttime in comparison with daytime, likely due to the fact that PAR, the dominant ET driver in the daytime, was typically not influenced by the tides. Our study also illustrated that the semidiurnal, spring-neap, and annual tidal cycles exerted strong effects on ET variations, which is indicated by the significant interactions between TWL and ET at diel, multiday, and seasonal timescales.

Different from inland ecosystems, the onshore or offshore wind direction heavily affected air mass conditions, thereby playing an important role in ET and energy processes at the coastal saltmarsh ecosystem in May-October, mainly due to the thermal contrast and air humidity difference between land and sea. We observed marked inhibitory effects of high tides on daytime ET under offshore wind conditions during May-October, indicating the non-negligible role of tidal inundation in regulating ET. The impacts of tidal flooding on ET can be made directly through regulating plant stomatal conductance or water and energy availability, and indirectly through modulating

micrometeorological conditions (e.g., VPD and T_a). This study stresses the uniqueness of coastal ecosystems that are subject to subdaily tides in ET processes and their environmental controls, and leads to better understanding of the mechanism of global ET variation, a benefit to realistic parameterization of ESMs and accurate prediction of water, carbon and energy cycles.

Supplementary materials

Supplementary material associated with this article can be found, in the online version, at doi:10.1016/j.agrformet.2019.107755.

References

Admiral, S.W., Lafleur, P.M., Roulet, N.T., 2006. Controls on latent heat flux and energy partitioning at a peat bog in eastern Canada. Agric. For. Meteorol. 140 (1), 308–321.

Admiral, S.W., Lafleur, P.M., 2007. Partitioning of latent heat flux at a northern peatland. Aquat. Bot. 86 (2), 107–116.

Baldocchi, D.D., 2003. Assessing the eddy covariance technique for evaluating carbon dioxide exchange rates of ecosystems: past, present and future. Glob. Chang Biol. 9 (4), 479–492.

Baldocchi, D., 2014. Measuring fluxes of trace gases and energy between ecosystems and the atmosphere – the state and future of the eddy covariance method. Glob. Chang Biol. 20 (12), 3600–3609.

Banach, K., 2009. Differences in flooding tolerance between species from two wetland habitats with contrasting hydrology: implications for vegetation development in future floodwater retention areas. Ann. Bot. 2 (103).

Bezerra, B.G., da Silva, B.B., Bezerra, J.R.C., Sofiatti, V., dos Santos, C.A.C., 2012. Evapotranspiration and crop coefficient for sprinkler-irrigated cotton crop in Apodi Plateau semiarid lands of Brazil. Agric. Water Manag. 107, 86–93.

Burba, G.G., Verma, S.B., Kim, J., 1999a. A comparative study of surface energy fluxes of three communities (*Phragmites australis, Scirpus acutus*, and open water) in a prairie wetland ecosystem. Wetlands 19 (2), 451–457.

Burba, G.G., Verma, S.B., Kim, J., 1999b. Surface energy fluxes of *Phragmites australis* in a prairie wetland. Agric. For. Meteorol. 94 (1), 31–51.

Chen, S., et al., 2009. Energy balance and partition in Inner Mongolia steppe ecosystems with different land use types. Agric. For. Meteorol. 149 (11), 1800–1809.

Clement, R., 1999. (http://www.geos.ed.ac.uk/abs/research/micromet/EdiRe).

Cornish, C.R., Bretherton, C.S., Percival, D.B., 2006. Maximal overlap wavelet statistical analysis with application to atmospheric turbulence. Boundary Layer Meteorol. 119 (2), 339–374.

Dolman, A.J., Miralles, D.G., de Jeu, R.A.M., 2014. Fifty years since Monteith's 1965 seminal paper: the emergence of global ecohydrology. Ecohydrology 7 (3), 897–902.

Eichelmann, E., et al., 2018. The effect of land cover type and structure on evapotranspiration from agricultural and wetland sites in the Sacramento–San Joaquin River Delta, California. Agric. For. Meteorol. 256-257, 179–195.

Fraser, A. and Swinney, H., 1986. Independent coordinates for strange attractors from mutual information, 33, 1134-1140 pp.

Fisher, J.B., et al., 2017. The future of evapotranspiration: global requirements for ecosystem functioning, carbon and climate feedbacks, agricultural management, and water resources. Water Resour. Res. 53 (4), 2618–2626.

Foken, T., Wichura, B., 1996. Tools for quality assessment of surface-based flux measurements. Agric. For. Meteorol. 78 (1), 83–105.

Forbrich, I., Giblin, A.E., 2015. Marsh-atmosphere CO2 exchange in a New England salt marsh. J. Geophys. Res. 120 (9), 1825–1838.

Ge, Z.-.M., et al., 2016. Spatiotemporal patterns of the gross primary production in the salt marshes with rapid community change: a coupled modeling approach. Ecol. Modell. 321, 110–120.

Goulden, M.L., Litvak, M., Miller, S.D., 2007. Factors that control Typha marsh evapotranspiration. Aquat. Bot. 86 (2), 97–106.

GSCCI (Group of Shanghai Coastal Comprehensive Investigation), 1988. Report of Shanghai Coastal Comprehensive Investigation. Shanghai Scientific and Technological Press, pp. 390.

Gu, S., et al., 2008. Characterizing evapotranspiration over a meadow ecosystem on the Qinghai-Tibetan Plateau. J. Geophys. Res. 113 (D8), D08118.

Guo, H., et al., 2009. Tidal effects on net ecosystem exchange of carbon in an estuarine wetland. Agric. For. Meteorol. 149 (11), 1820–1828.

Guo, H., et al., 2010. Seasonal changes of energy fluxes in an estuarine wetland of Shanghai, China. Chin. Geograph. Sci. 20 (1), 23–29.

Han, G., et al., 2015. Effects of episodic flooding on the net ecosystem CO2 exchange of a supratidal wetland in the Yellow River Delta. J. Geophys. Res. 120 (8), 1506–1520.

Harazono, Y., et al., 1998a. Measurement of energy budget components during the International Rice Experiment (IREX) in Japan. Hydrol. Process. 12 (13–14), 2081–2092.

Harazono, Y., Yoshimoto, M., Mano, M., Vourlitis, G.L., Oechel, W.C., 1998b. Characteristics of energy and water budgets over wet sedge and tussock tundra ecosystems at North Slope in Alaska. Hydrol. Process. 12 (13–14), 2163–2183.

Hollinger, D., Richardson, A., 2005. Uncertainty in eddy covariance measurements and its application to physiological models. Tree Physiol. 25, 873–885.

Hurrell, J.W., et al., 2013. The community earth system model: a framework for collaborative research. Bull. Am. Meteorol. Soc. 94 (9), 1339–1360.

Igarashi, Y., et al., 2015. Environmental control of canopy stomatal conductance in a tropical deciduous forest in northern Thailand. Agric. For. Meteorol. 202, 1–10.

Jung, M., et al., 2010. Recent decline in the global land evapotranspiration trend due to limited moisture supply. Nature 467 (7318), 951–954.

Kaimal, J.C., Gaynor, J.E., 1991. Another look at sonic thermometry. Boundary Layer Meteorol. 56 (4), 401–410.

Kaimal, J.C., Finnigan, J.J., 1994. Atmospheric Boundary Layer flows: Their Structure and Measurement. Oxford University Press, New York.

Kathilankal, J.C., et al., 2008. Tidal influences on carbon assimilation by a salt marsh. Environ. Res. Lett. 3 (4), 044010.

Kathilankal, J.C., et al., 2011. Physiological responses of Spartina alterniflora to varying environmental conditions in Virginia marshes. Hydrobiologia 669 (1), 167–181.

Katul, G.G., Oren, R., Manzoni, S., Higgins, C., Parlange, M.B., 2012. Evapotranspiration: a process driving mass transport and energy exchange in the soil-plant-atmosphere-climate system. Rev. Geophys. 50 (3), RG3002.

Kirwan, M.L., Megonigal, J.P., 2013. Tidal wetland stability in the face of human impacts and sea-level rise. Nature 504 (7478), 53–60.

Kljun, N., Calanca, P., Rotach, M.W., Schmid, H.P., 2004. A simple parameterisation for flux footprint predictions. Boundary Layer Meteorol 112 (3), 503–523.

Kljun, N., Calanca, P., Rotach, M.W., Schmid, H.P., 2015. A simple two-dimensional parameterisation for Flux Footprint Prediction (FFP). Geosci. Model Dev. 8 (11), 3695–3713.

Knox, S.H., Windham-Myers, L., Anderson, F., Sturtevant, C., Bergamaschi, B., 2018. Direct and indirect effects of tides on ecosystem-scale CO2 exchange in a Brackish Tidal marsh in Northern California. J. Geophys. Res. 123 (3), 787–806.

Lei, H., Yang, D., 2010. Interannual and seasonal variability in evapotranspiration and energy partitioning over an irrigated cropland in the North China Plain. Agric. For. Meteorol. 150 (4), 581–589.

Lettenmaier, D.P., Famiglietti, J.S., 2006. Hydrology: water from on high. Nature 444 (7119), 562–563.

Li, B., et al., 2009. Spartina alterniflora invasions in the Yangtze River estuary, China: an overview of current status and ecosystem effects. Ecol. Eng. 35 (4), 511–520.

Liljedahl, A.K., et al., 2011. Nonlinear controls on evapotranspiration in arctic coastal wetlands. Biogeosciences 8 (11), 3375–3389.

Mahrt, L., 1998. Flux sampling errors for aircraft and towers. J. Atmos. Ocean. Technol. 15 (2), 416–429.

Ma, N., et al., 2015. Environmental and biophysical controls on the evapotranspiration over the highest alpine steppe. J. Hydrol. 529 (Part 3), 980–992.

Malone, S.L., et al., 2014. Seasonal patterns in energy partitioning of two freshwater marsh ecosystems in the Florida Everglades. J. Geophys. Res. 119 (8), 1487–1505.

Moffett, K.B., Wolf, A., Berry, J.A., Gorelick, S.M., 2010. Salt marsh–atmosphere

exchange of energy, water vapor, and carbon dioxide: effects of tidal flooding and biophysical controls. Water Resour. Res. 46 (10), W10525.

Monteith, J.L., Unsworth, M.H., 2013. Chapter 3 - Transport of heat, mass, and momentum. In: Monteith, J.L., Unsworth, M.H. (Eds.), Principles of Environmental Physics, fourth ed. Academic Press, Boston, pp. 25–35.

Moore, P.A., Pypker, T.G., Waddington, J.M., 2013. Effect of long-term water table manipulation on peatland evapotranspiration. Agric. For. Meteorol. 178–179, 106–119.

Moore, C.J., 1986. Frequency response corrections for eddy correlation systems. Boundary Layer Meteorol. 37 (1), 17–35.

Nicolini, G., et al., 2017. Performance of eddy-covariance measurements in fetch-limited applications. Theor. Appl. Climatol. 127 (3), 829–840.

Odongo, V.O., et al., 2016. Energy partitioning and its controls over a heterogeneous semi-arid shrubland ecosystem in the Lake Naivasha Basin, Kenya. Ecohydrology 9 (7), 1358–1375.

Office of Shanghai Chronicles, 2003. Climate Available at: http://www.shtong.gov.cn/ Newsite/node2/node4/node2250/node4426/node16046/node16130/index.html Accessed: 22 August 2019.

Qiu, G.Y., Xie, F., Feng, Y.C., Tian, F., 2011. Experimental studies on the effects of the "Conversion of Cropland to Grassland Program" on the water budget and evapotranspiration in a semi-arid steppe in Inner Mongolia, China. J. Hydrol. 411 (1), 120–129.

Reichstein, M., et al., 2005. On the separation of net ecosystem exchange into assimilation and ecosystem respiration: review and improved algorithm. Glob. Chang. Biol. 11 (9), 1424–1439.

Raupach, M.R., 1995. Vegetation-atmosphere interaction and surface conductance at leaf, canopy and regional scales. Agric. For. Meteorol. 73 (3), 151–179.

Ruddell, B.L., Sturtevant, C., Kang, M., and Yu, R. (2008). ProcessNetwork Software, version 1.5. Accessed as https://ww2.mathworks.cn/matlabcentral/fileexchange/ 41515-processnetwork-processnetwork_software on 21 March 2016.

Stoy, P.C., et al., 2013. A data-driven analysis of energy balance closure across FLUXNET research sites: the role of landscape scale heterogeneity. Agric. For. Meteorol. 171-172, 137–152.

Sturtevant, C., et al., 2016. Identifying scale-emergent, nonlinear, asynchronous processes of wetland methane exchange. J. Geophys. Res. 121 (1), 188–204.

Sun, S., Cai, Y., Liu, H., 2001. Biomass allocation of Scirpus mariqueter along an elevational gradient in a salt marsh of the Yangtse River estuary. Acta Bot. Sin. 43 (2), 178–185.

Tang, J., et al., 2006. Sap flux–upscaled canopy transpiration, stomatal conductance, and water use efficiency in an old growth forest in the Great Lakes region of the United States. J. Geophys. Res. 111 (G2).

Unland, H.E., Houser, P.R., Shuttleworth, W.J., Yang, Z.-.L., 1996. Surface flux measurement and modeling at a semi-arid Sonoran Desert site. Agric. For. Meteorol. 82 (1), 119–153.

Wagle, P., et al., 2015. Biophysical controls on carbon and water vapor fluxes across a grassland climatic gradient in the United States. Agric. For. Meteorol. 214–215, 293–305.

Webb, E.K., P, G.I., L, R., 1980. Correction of flux measurements for density effects due to heat and water vapour transfer. Q. J. R. Meteorol. Soc. 106 (447), 85–100.

Wilson, K., et al., 2002. Energy balance closure at FLUXNET sites. Agric. For. Meteorol. 113 (1–4), 223–243.

Wilson, K.B., Baldocchi, D.D., 2000. Seasonal and interannual variability of energy fluxes over a broadleaved temperate deciduous forest in North America. Agric. For. Meteorol. 100 (1), 1–18.

Yang, S.-l., Ding, P.-x., Chen, S.-l., 2001. Changes in progradation rate of the tidal flats at the mouth of the Changjiang (Yangtze) River, China. Geomorphology 38 (1), 167–180.

Zhu, G., et al., 2014. Energy flux partitioning and evapotranspiration in a sub-alpine spruce forest ecosystem. Hydrol. Process. 28 (19), 5093–5104.

Zhou, S., Yu, B., Huang, Y., Wang, G., 2015. Daily underlying water use efficiency for AmeriFlux sites. J. Geophys. Res. 120 (5), 887–902.

Zhao, B., Gao, Y., 2018. Changjiang Estuary Wetland. China Agriculture Press, Beijing.